RSC Advances




ROYAL SOCIETY OF CHEMISTRY

www.rsc.org/advances

RSC Advances

ARTICLE

# One-step synthesis of $Bi_2WO_6/Bi_2O_3$ loaded reduced graphene oxide multicomponent composite with enhanced visible-light photocatalytic activity

Received 00th January 20xx,
Accepted 00th January 20xx

DOI: 10.1039/x0xx00000x

www.rsc.org/

Shuang Zhong[a], Fengjun Zhang[a], Wei Lu[a], Tianye Wang*[a] and Liyuan Qu[a]

In this study, the characterization and photocatalytic activity of $Bi_2WO_6/Bi_2O_3$ loaded reduced graphene oxide under visible-light irradiation was investigated in detail. The results suggested that the $Bi_2WO_6/Bi_2O_3$ loaded reduced graphene oxide can be synthesized by a facile one-step solvothermal process. Through the characterization of the composite photocatalyst by X-ray diffraction, scanning electron microscopy, Transmission electron microscopy, X-ray photoelectron spectroscopy, Fourier transform infrared, UV-vis diffuse reflectance spectra and Photoluminescence spectra, it was found that $Bi_2WO_6/Bi_2O_3$@RGO composite was formed, meanwhile GO was completely reduced to graphene and bonded with $Bi_2WO_6/Bi_2O_3$ with by C-O to form composite. The as-prepared composite owned enhanced absorption in the UV to visible-light region and exhibited decreased radiative recombination of photogenerated charge carriers. Moreover, it was expected that the as-prepared composites exhibited enhanced photocatalytic activity for the degradation of Rhodamine B under visible-light irradiation. Among them, BWO@R3 (GO%=5%) owned the best photocatalytic activity, which can photodegrade RhB ($10^{-2}$ g/L) reaching 99.6% in 20min and high concertration RhB ($30^{-2}$ g/L) reaching 99.2% in 180 min. It can be ascribed to their improved light absorption property and the reduced recombination of the photogenerated electron-holes during the photocatalytic reaction.

## 1. Introduction

Among the novel photocatalysts, the multicomponent metal oxides containing bismuth are regarded as excellent visible-light-driven photocatalysts[1, 2]. Very recently, $Bi_2WO_6$ with high visible-light responsivity has been widely investigated by many teams in the field of photocatalysis[3, 4]. $Bi_2WO_6$ as one of the simple members of the Aurivillius family is composed of accumulated layers of coner-sharing $WO_6^{2+}$ octahedral sheets and bismuth oxide sheet [5], and it has been found that $Bi_2WO_6$ exhibits the highest photocatalytic activity among the above $Bi^{3+}$-based oxides under visible-light irradiation [6, 7].

However, the slow electron transfer and highly efficient electron-hole recombination limits its applications in photocatalysis has greatly limited[8]. To overcome these drawbacks, it is essential to improve the charge separation efficiency and extend the spectral responsive range for real applications in the environment. Among the various studies for modifying $Bi_2WO_6$, $Bi_2WO_6/Bi_2O_3$ [9, 10, 11] as the typical p-n composite photocatalysts with narrow bandgap and improved charge separation efficiency get more attention. However, there are still some drawbacks, such as the limited region of visible-light photoresponse and the highly efficiency of electron-hole recombination prohibits the desirable catalytic activity under visible-light irradiation[12, 13]. To solve these problems, multicomponentcomposite have been developed[14, 15, 16], in which two or more visible-light active components and an electron-transfer system are spatially integrated[13, 17], such as S-$Bi_2WO_6/Bi_2O_3$[4] . S-$Bi_2WO_6/Bi_2O_3$ exhibited enhanced photocatalytic activity for RhB under visible-light irradiation and decreased recombination of photogenerated charge carriers, however the composite did not own well adsorbability and practicability. Hence, in order to further enhance the stability $Bi_2WO_6/Bi_2O_3$ adsorbability for the practical application, the functional material is chosen to integrate into $Bi_2WO_6/Bi_2O_3$.Graphene has a perfect $sp^2$-hybridized two dimensional carbon structure with excellent conductivity and large surface area[2], so that graphene owns excellent electron conductivity and high adsorption[18]. Hence, graphene-modified semiconductor nanocomposites were regarded as novel photocatalysts for degradation of pollutants[19-21] . For ideal graphene-semiconductor photocatalysts, semiconductors should be loaded firmly onto the surface of the individual two-dimensional sheets of graphene, which will maximize the utilization of electron conductivity of graphene[22, 23].

Nevertheless, several works investigating[2, 23-26] the preparation and properties of bismuth tungstate– graphene composite materials showed that photocatalytic activity is enhanced in the composite photocatalysts. However, so far, these composite photocatalysts were prepared by a two-step method or the synthesis amount was little, which were inconvenient for the practical application. The purpose in this study is to find a more convenient method to prepare bismuth tungstate–graphene composite photocatalysts[27] .

[a] Key Laboratory of Groundwater Resources and Environment, Ministry of Education, Jilin University, Changchun 130026, China. E-mail: wangtianye11@hotmail.com

Based on the above theories and through modification of preparation conditions, $Bi_2WO_6/Bi_2O_3$-loaded reduced graphene oxide (RGO) composite phtotocatalysts with high photocatalytic activity were prepared via a one-step solvothermal process. During the preparation, graphene oxide (GO) was directly reduced without secondary reduction. This route is simple and highly productive, so that the determined experimental parameters are more suitable for the actual mass production.

## 2. Materials and methods

### 2.1 Materials

$Bi(NO_3)_3{\cdot}5H_2O$ was purchased from Guangdong Xilong Chemical Co., Ltd. $Na_2WO_4{\cdot}2H_2O$ were purchased from Shanghai Chemical Company. Sodium oleate, ethylene glycol (EG) and ethyl alcohol were purchased from Sinopharm Chemical Reagent Co., Ltd. All chemicals were analytical reagent grade without further purification.

Graphene oxide (GO) was synthesized according to the modification of Hummers' methods and the process was described previously[28].

### 2.2 Synthesis of $Bi_2WO_6/Bi_2O_3$@RGO

Sodium oleate (4mmol) and $Bi(NO_3)_3{\cdot}5H_2O$ (4mmol) were successively dissolved to 40mL ethylene glycol, at the same time an appropriate mass ratio of GO (GO% = 1%, 2%, 5%, 10%) was ultrasonically dissolved in 20 mL ethylene glycol, and then the two solution were mixed together and stired 0.5h. 20mL ethylene glycol dissolved with $Na_2WO_4{\cdot}2H_2O$ (4mmol) was then injected into the above mixture solution. After vigorous stirring for 2h, the mixture was transferred to a 100mL Teflon-lined autoclave, sealed, and heated at 180°C for 20h. After that, the system was cooled down to room temperature. Then, the solid precipitate were filtered and washed with the distilled water and ethyl alcohol for three times. The products were dried at 60°C for 12h. The solids were ground, and then black powdered $Bi_2WO_6/Bi_2O_3$ loaded RGO multicomponent composite (abbreviation as BWO@R1-4) were prepared. For comparison, $Bi_2WO_6/Bi_2O_3$ (abbreviation as BWO) without RGO was also prepared as contrast sample.

The abbreviations of as-prepared composites according to the different GO% were listed in Table1.

Table 1 $Bi_2WO_6/Bi_2O_3$@RGO composite with the different GO%

| BWO@R | BWO | BWO@R 1 | BWO@R 2 | BWO@R 3 | BWO@R 4 |
|---|---|---|---|---|---|
| GO% | 0 | 1% | 2% | 5% | 10% |

### 2.3 Characterization

X-ray diffractometry (XRD) was conducted by a Japan Rigaku Rotaflex diffractometer with a monochromatic Cu Kα radiation source, under 40 kV and 100 mA (λ = 0.15418 Å). Scanning electron microscopy (SEM) images were observed by a JEOLJSM-6700F SEM device. The energy-dispersive X-ray spectroscopy (EDS) was also performed during the SEM measurement. Transmission electron microscopy (TEM) was recorded on a FECNAI F20 microscope. X-ray photoelectron spectroscopy (XPS) measurement was carried out by an ESC ALAB-250I-XL device. Fourier transform infrared spectra (FT-IR) were recorded by a Nicolet 500 FT-IR analyzer using KBr pellets in the region 4000–400 $cm^{-1}$. Ultraviolet-visible diffuse reflectance spectra (UV-DRS) were recorded by a UV-visible spectrophotometer (TU-1901) using $BaSO_4$ as a reference. Photoluminescence (PL) spectra were measured on a Hitachi F-4600 fluorescence spectrophotometer (λEx=338 nm) at room temperature. Electron spin resonance (ESR) signals of radicals spin-trapped by 5,5-dimethyl-1-pyrroline N-oxide (DMPO) were recorded at room temperature on a JES FA200 spectrometer.Mott-Schottky plots were measured using a three-electrode CHI660E electrochemical workstation at a fixed frequency of 1 kHz in 0.5 M $Na_2SO_4$ solution.

### 2.4 Photocatalytic test

Photocatalytic activities of the as-prepared composites were evaluated via the photodegradation of RhB under the irradiation of a 500 W Xe lamp in a sealed photocatalytic reactor. In each experiment, 1.00 g/L of catalyst was added to the RhB solution (10 mg/L). Before irradiation, the solution was stirred for 75 min in the dark to reach adsorption-desorption equilibrium. After that, the mixture solution containing the photocatalyst and RhB was placed under the Xe lamp. At each time interval, a 3.5 mL mixture was sampled and centrifuged to remove the photocatalyst particles. Then the UV-visible absorbance of the centrifuged solution was recorded by UV-visible spectrophotometer.

## 3. Results and discussion

### 3.1 Characterization of the catalysts

The phase and composition of BWO@R were characterized by XRD, as shown in Figure 1. All diffraction peaks of the as-prepared composites can be well indexed to the standard phase-pure orthorhombic $Bi_2WO_6$ (a=5.457 Å, b=16.435 Å, c=5.438 Å, JCPDS No. 39-0256) and cubic $Bi_2O_3$ (a=b=c= 5.450 Å, JCPDS No. 76-2478). It suggested that $Bi_2WO_6/Bi_2O_3$ composite photocatalyst was synthesized in the solvothermal process[9]. However, no characteristic diffraction peak for graphene was observed in the patterns. It is attributed to the relatively low amount and diffraction intensity of graphene compared with that of $Bi_2WO_6/Bi_2O_3$. The conclution is consistent with some literatures [15, 25, 27]. These results indicated that new catalyst was not formed and the original crystal form was not changed by loading RGO [28]. However, it was shown that the intensity of the diffraction peaks of the composite photocatalysts were reduced due to loading RGO. It indicated that the crystallinity of BWO@R was weakened due to the covering of RGO [23].

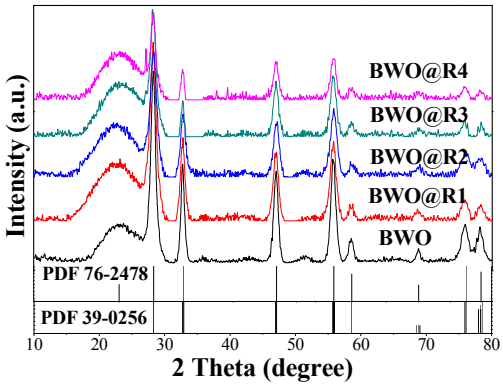


**Figure 1** The XRD patterns of BWO@R multiple composite with the different GO%

The crystallite size of the composite photocatalysts were estimated using the Scherrer equation[23, 29] :

$$D=K\lambda/B\cos\vartheta \quad (1)$$

where D is crystallite size; B is full width at half-maximum (FWHM); K is Scherrer constant 0.89; λ=0.154056 nm, which is X-ray wavelength; θ is the angle of diffraction[30]. By calculating with the peaks which had the largest peak areas in XRD, the crystallite size of the as-prepared composites were 8.6 of BWO@R1, 5.2 of BWO@R2, 5.4 of BWO@R3, 13.7 of BWO@R4 and 8.8 of BWO. The results show that the lattice dimensions of BWO@R is effectively reduced due to loading RGO. It is attributed to that the crystal growth of $Bi_2WO_6/Bi_2O_3$ is suppressed by the spatial isolation effect of graphene [23]. It is obvious that the lattice dimensions of BOW@R2 (GO%=2%) is the smallest amoung the as-prepared composites. However, the lattice dimension significantly increases due to too excessive addition of RGO (GO%=10%). It is presumed that the agglomeration of the particles occurred by the excess of RGO[23].

Table 2. The Crystallite Size of BWO@R

| Samples | BWO | BWO @R1 | BWO@ R2 | BWO@ R3 | BWO@ R4 |
|---|---|---|---|---|---|
| Lattice dimensions (nm) | 8.8 | 8.6 | 5.2 | 5.4 | 13.7 |

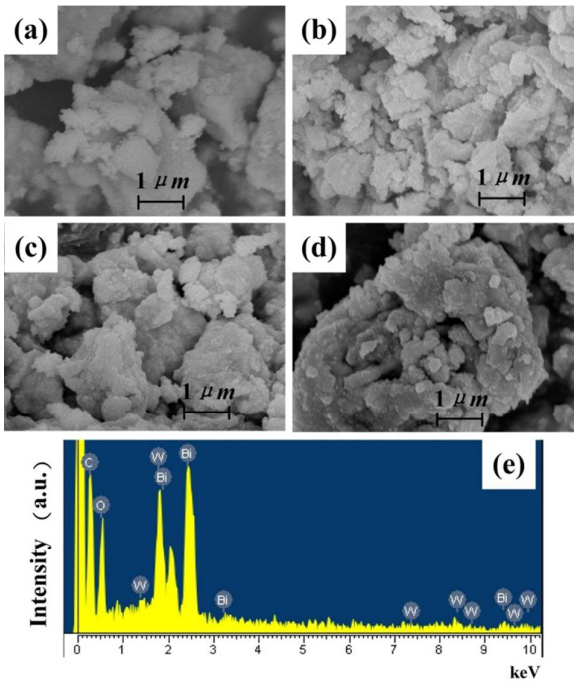


**Figure 2** SEM images of BWO@R with the different GO% (a)BWO@R1; (b) BWO@R2; (c) BWO@R3; (d) BWO@R4; (e) EDS spectra of BWO@R3

The appearances of BWO@R were observed by SEM, as shown in Figure 2. It is obvious that BWO@R is piled up to a sheet-shape, which is consistent with the special sheet-like structure of graphene. It indicates that Bi2WO6/Bi2O3 is successfully loaded onto the surface of RGO. There is a grain-like structure rather than a evident sheet-like structure at GO% = 1%, which is likely to results from the low dosage(Fig. 2a). With further increase of GO%, the sheet-like structure is increasingly evident (Fig. 2b, 2c). It is the most evidently that BWO@R2 disperses with the smallest size and the thinnest sheet at GO% = 2% , which indicates the modest dispersing effect of the GO[23]. However, it is shown obviously that the agglomeration of BWO@R4 occurs at GO%=10% due to the excess of RGO, which is probably attributed to that GO could not be dispersed well in the solution by the excessive dosage (Fig. 2d). Meanwhile, C, Bi, W and O were confirmed as major elements in BWO@R by EDX elemental microanalysis, which indicates that RGO existed in the composite photocatalyst.

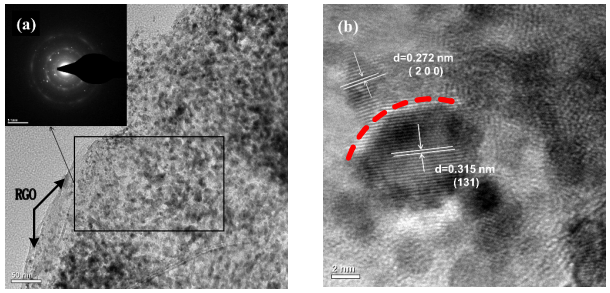


**Figure 3** (a)TEM images and inserted SAED pattern of BWO@R2

(b)high-resolution image with the magnification of the $Bi_2WO_6$ and $Bi_2O_3$ lattice

The microstructure of BWO@R2 was further investigated by TEM and high resolution TEM(HRTEM), as shown in Figure 4. The 2D graphene sheets and $Bi_2WO_6/Bi_2O_3$ nanoparticles are clearly observed in Figure 3(a). The well-crystallized $Bi_2WO_6/Bi_2O_3$ nanoparticles present on the surface of graphene sheets, which is illustraed by characteristic wrinkles on the edge. The selected area electron-diffraction (SEAD) pattern (Fig.3(a)) reveals that $Bi_2WO_6/Bi_2O_3$ is polycrystalline nature ingredient in BWO@R2 . From the HRTEM image of BWO@R (Fig. 3(b)), it is illustrated that a set of clear lattice fringes with the interspacing of 0.315 nm corresponding to the (131) crystal plane of orthorhombic $Bi_2WO_6$ and 0.272nm corresponding to the (200) crystal plane of cubic phase $Bi_2O_3$ are found, which are consistent with the lattices that were calculated by Bragg equation in XRD. Furthermore, an interconnected well nanoparticulate morphology is observed, indicating that heterojunctions were formed in the composite photocatalyst[8]. The well-defined fringes and the high crystallinity of BWO@R2 can facilitate the separation of the photogenerated carriers, improving the corresponding photocatalytic activities[29, 31].

The surface element composition and the chemical states of all elements were analyzed with XPS, as shown in Figure. 4. The chemical states of Bi, W, O and C in BWO@R were investigated, as well as the reduction state of organic carbon in RGO. The full spectrum spectra of BWO@R2 shows that C 1s, O 1s, Bi 4f and W 4f are all presented in the as-prepared composites (Fig. 3a). The XPS spectra of C 1s (Fig. 3b) shows the reductive degree of organic carbon in RGO of BWO@R2 during the preparation. The C1s of GO shows four XPS peaks, which correspond to the C-C in non-oxidative carbon (284.6 eV), C-O in epoxy and hydroxy (286.99 eV), C=O in carbonyl (288.95 eV), and O-C=O in carboxyl (290.46 eV)[32] , indicating that GO contains abundant C and O organic groups. The XPS spectra of C1s in BWO@R2 shows that the characteristic peaks of C-O, C=O and O-C=O basically disappeared, but the characteristic peak of C-C almost did not change. These results indicate that the organic groups of C and O were reduced during the preparation, and the GO in BWO@R was reduced to graphene. Compared with C-O from GO, the peak of C-O in BWO@R migrated to lower binding energy, indicating that GO interacted with $Bi_2WO_6/Bi_2O_3$ by C-O to form BWO@R composite [2]. The XPS spectra of O1s from the BWO@R2. The XPS spectra of O1s from the BWO@R2 (Fig. 3c) can be deconvoluted the two peaks representing O1s in $Bi_2WO_6$ (530.29) and $Bi_2O_3$ (532.2 eV), but the two peaks are neither consistent with the peaks of O1s in GO. These results further indicates that the O-containing groups in GO were reduced. In conclusion, during the synthesis of BWO@R, ethylene glycol with sodium oleate can enhanced the reduction reaction so that GO can be completely reduced to graphene. Moreover, graphene bonded with $Bi_2WO_6/Bi_2O_3$ with by C-O to form BWO@R composite.

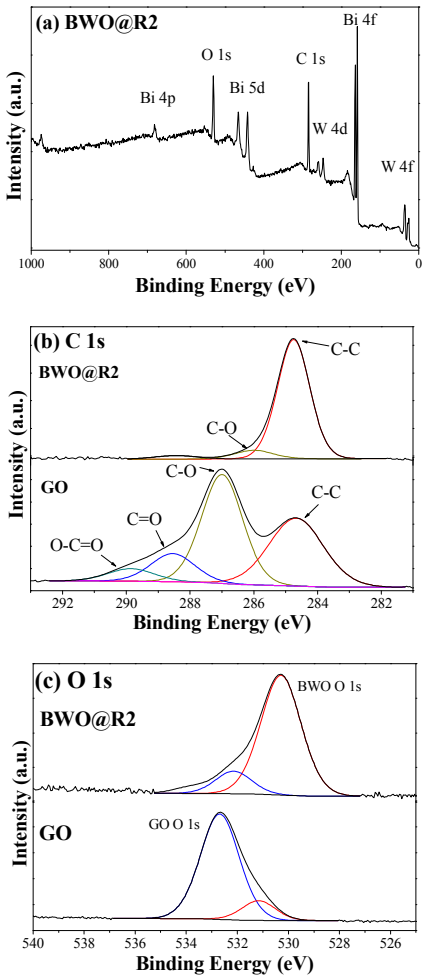


**Figure 4** XPS spectra of BWO@R3 composite and GO (a) Survey spectra; (b) C 1s; (c) O 1s

The oxygen-containing groups and chemical interaction of BWO@R was illustrated by FT-IR spectra, as shown in Figure. 5. The absorption peaks at 400-1100 $cm^{-1}$ are attributed to bridging stretching modes of metal-O [33, 34], in this range the peak at 489 $cm^{-1}$ is related to the stretching vibration of Bi-O [30], and the peaks at 569 and 727 $cm^{-1}$ are attributed to the stretching vibration of $WO_6$ in $Bi_2WO_6$ [35]. It is found that the absorption peaks positions were not significantly different among all catalysts, nevertheless there were some differences at 1520 $cm^{-1}$, 1615 $cm^{-1}$ and 1079 $cm^{-1}$. The IR absorption of the peaks at 1615 and 1079 $cm^{-1}$ decreased with the increasing amount of GO, which is associated with the decreasing of the stretching vibration mode of C=O on the surface of the as-prepared composites [14, 32, 36]. However, the IR absorption of the peaks at 1520 $cm^{-1}$ rose with the increasing amont of GO, which indicates that the simple substance carbon species increased on the as-prepared heterojuncions [34]. These suggeste that GO be reduced to graphene in the reaction system, of which C=O be mainly reduced to the simple substance carbon species. This further confirmed the XPS analysis.

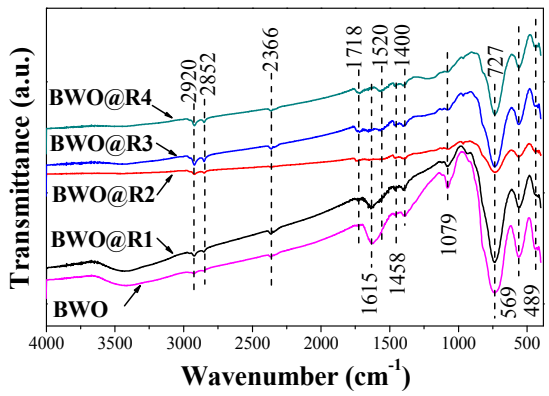


**Figure 5** FT-IR spectra of (a) BWO@R；(b) BWO@R2 after adsorption and photocatalysis of RhB

The UV-vis diffuse-reflectance spectrum revealed that the absorption edge of $Bi_2WO_6/Bi_2O_3$ extended to the visible-light region, as shown in Figure 6, which implied the possibility of enhanced photocatalytic activity of these materials under visible-light irradiation. According to the spectra, all BWO@R exhibit high UV-vis absorbance, which indicate that the as-prepared composites possess the high UV-vis responses[27]. Within the visible range (400-800 nm), however, BWO@R exhibits higher absorbance than BWO, indicating that the loading RGO can enhanced the visible-light response of the as-prepared composites. The reasons are that black body properties typical of graphite-like materials own enhance absorption intensity, and meanwhile the reintroduction of graphite can modify the original formation of photoelectrons-holes[28]. Moreover, graphene as a visible-light sensitizing agent can broaden the absorption range under visible-light [24]. The steep lines in the graphs indicate that the enhancement of visible-light response is attributed to the energy level transition rather than the impurity transition [5]. These results also indicate that the charge carrier inside BWO@R occurred the energy level transition, which can enhanced the range of visible-light adsorbability.

For a crystalline semiconductor, the band gap energy of a semiconductor can be calculated by the Kubelka-Munk equation [8, 37, 38]:

$$\alpha h\nu = A(h\nu - E_g)^{n/2} \qquad (2)$$

where, $\alpha$ *is* the absorption coefficient, *h* is the Planck constant, *v is* the light frequency, $E_g$ is the band gap, and A is a constant. Among them, n is determined from the type of optical transition of a semiconductor, and the value of n for the direct semiconductor ($Bi_2WO_6$) is 1[39]. The band gaps were estimated from the $(\alpha h\nu)^2$ versus photon energy ($h\nu$) plots were 2.60 eV (BWO@R1), 2.28 eV (BWO@R2), 1.87 eV (BWO@R3), 2.61eV (BWO@R4), respectively, as shown in the Figure 6(b). It is obviously shown that the band gap of BWO@R3 (GO%=5%) is the smallest, suggesting that loading RGO can effectively shorten the gap band of the as-prepared composites. Meanwhile, it illustrated that the separation and migration of photogenerated carriers are improved by the high conductibility of RGO. Hence, loading RGO can enhance the visible-light response and photogenerated carriers transfer of the composites.

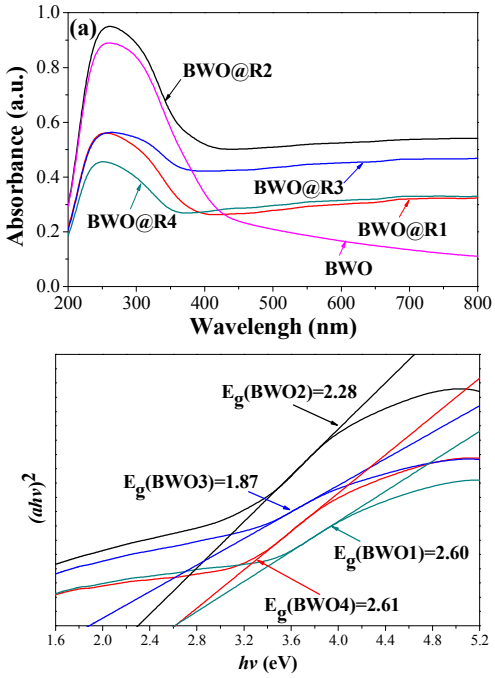


**Figure 6** (a) UV-vis DRS spectra of BWO@R multiple composite with the different GO% (b) estimated band gap by Kubelka-Munk function

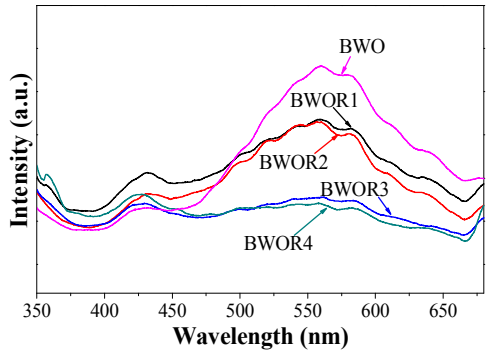


**Figure 7** Room-temperature PL spectra of BWO@R composite with the different GO%

The separation effciency of photogenerated charge carriers in $Bi_2WO_6/Bi_2O_3$ loaded RGO composites were surveyed by Photoluminescence spectra (excited at 300 nm), as shown in Figure 7. The PL emissions are originated from the radiative recombination of photogenerated electrons–holes[10, 40], thus a higher PL emission peak indicates that it is easier to combination of the charge carriers [41]. It is obvious that the intensity of the PL emission peaks of the as-prepared composites were dramatically weakened with the increase of GO%, and the PL peaks of BWO@R decrease as follows: BWO> BWO@R1> BWO@R2> BWO@R3≈BWO@R4. Therefore, these results indicate that the as-

prepared composites could more effectively inhibit the recombination of photogenerate charge carriers by loading RGO than that $Bi_2WO_6/Bi_2O_3$, and that the inhibiting abilities of BWO@R3 and BWOR4 were most strong. It indicats that loading RGO is the major reason for inhibiting combination of photogenerate electrons-holes. This is because graphene possesses superior properties, such as a unique two-dimensional layer structure and high electrical conductivity, as well as large specific surface area, which is beneficial to enhance separation efficiency of photogenerate charge carriers and inhibit recombination of photogenerate electrons-holes[18]. Thereby, the as-prepared composites can effectually enhanced the photocatalytic activity [28], further confirming the existence of covalent bonding interactions between RGO and BWO and smaller , which is consistent with the results of FT-IR and XPS[24]. Meanwhile, it was determined that BWO@R3 has the best ability to inhibit the recombination of photogenerate charge carriers, which was mateched by the resultof UV-DRS, indicating that BWO@R3 owns the best photocatalytic activity.

### 3.2 Photocatalyic activities

The adsorbed ability of BWO@R was tested by the adsorption of RhB under dark conditions, as showed in Figure 8. It is shown that the adsorption of RhB was enhanced in the presence of BWO@R2 compared with that of BWO, reaching 88.2% in 120 min. It illustrates obviously that loading of graphene significantly enhanced the adsorption of BWO@R3. This is because the two-dimensional planar structure and large conjugated π bond of graphene can make RhB molecules easily adsorb on the sureface of BWO@R3 via strong π-π conjugation interactions between graphene and RhB [26].

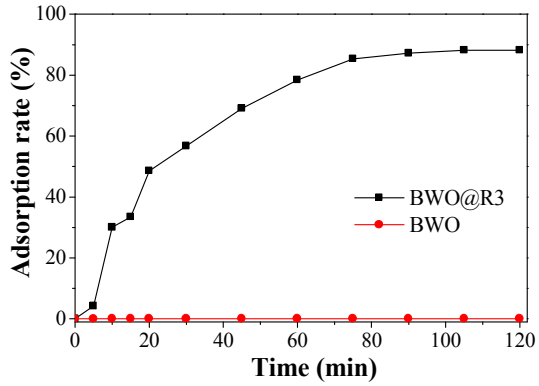


**Figure 8** The adsorption curve of RhB by BWO@R3 (BWO@R: 1.00g/L; RhB: $10^{-2}$ g/L)

The photocatalytic activities of BWO@R were evaluated by the degradation of RhB ($10^{-2}$ g/L) under visible-light irradiation, as showed in Figure 9(a). It is shown that BWO@R exhibited enhanced photocatalytic activity in degradation of RhB. Compared with the adsorption, the photocatalysis of BWO@R is mainly responsible for the degradation of RhB. It is obvious that BWO@R2 and BWO@R3 exhibited the highest photocatalytic activity with degradation ratio of RhB reaching 99.6% in 20min, followed by BWO@R4, BWO@R4 and BWO. The photocatalytic activity of the as-prepared composites in the study is significantly improved compared with that of $Bi_2WO_6/Bi_2O_3$ (degradation ratio 60% in 95 min). These results indicate that the loading RGO can evidently enhance the visible-light catalytic activity. The reasons are that with a typical large conjugated π bond and high conductibility, the combination of RGO with $Bi_2WO_6/Bi_2O_3$ can efficiently transfer the photoelectrons, inhibit its combination with holes, and largely enhance the photocatalytic activity of the composites[25]. The photocatalytic activity of the as-prepared composites in the study was significantly improved compared with that of $Bi_2WO_6/Bi_2O_3$ (degradation ratio 60% in 95 min). However, the photocatalytic activity of the corresponding BWO@R4 (GO%=10%) was less weakened than that of BWO@R2 (GO%=2%), probably because the excessive RGO covered the active centers of BWO@R4. Therefore, the optimal GO% in synthesis of BWO@R composites is determined to be 5%. In addition, in the same experimental condition, the photocatalytic activity of BWO@R3 is better than the results of the Bi2WO6/Bi2O3 composites that have been reported[4], which further indicated that the photocatalytic activity of the as-prepared composites in the study was better improved.

Meanwhile, the temporal evolution of the spectra during the photodegradation with BWO@R2 for RhB under visible-light irradiation (λ>420nm) was displayed in Figure. 9(b). A rapid decrease of RhB absorption at the wavelength of 553 nm was observed, and the spectral maximum shifted from 553 to 496 nm. The color of the suspension changed gradually from pink to light green, which is in agreement with the shift of the major absorption. The hypsochromic shifts were caused by the removal of the N-ethyl groups and the destruction of the conjugated structure from RhB during the photodegradation [42, 43]. It also proves that photochemical changes of RhB occurred by the as-prepared composite during the degradation process, rather than adsorption. After 20min reaction, the hypsochromic shifts of the absorption band were considerably insignificant. The major absorption peaks decreased sharply and the color was clear in the following photodegradation. It was inferred that the cleavage of the whole chromophore structure (cycloreversion) of RhB occurred over the photocatalysts [44, 45]. These indicated that the as-prepared composite exhibits excellent photocatalytic activity in the degradation of RhB.

In addition, the photodegradation of higher concentration RhB ($30^{-2}$ g/L) by BWO@R3 was shown in Figure 9(c) It is shown that BWO@3 also exhibited well photodegradation to high concentration RhB. The degradation ratio of RhB reached 99.2% in 180 min, which more obviously indicated that BWO@R3 possesses enhanced photocatalytic activity for RhB, even though in higher concentration.

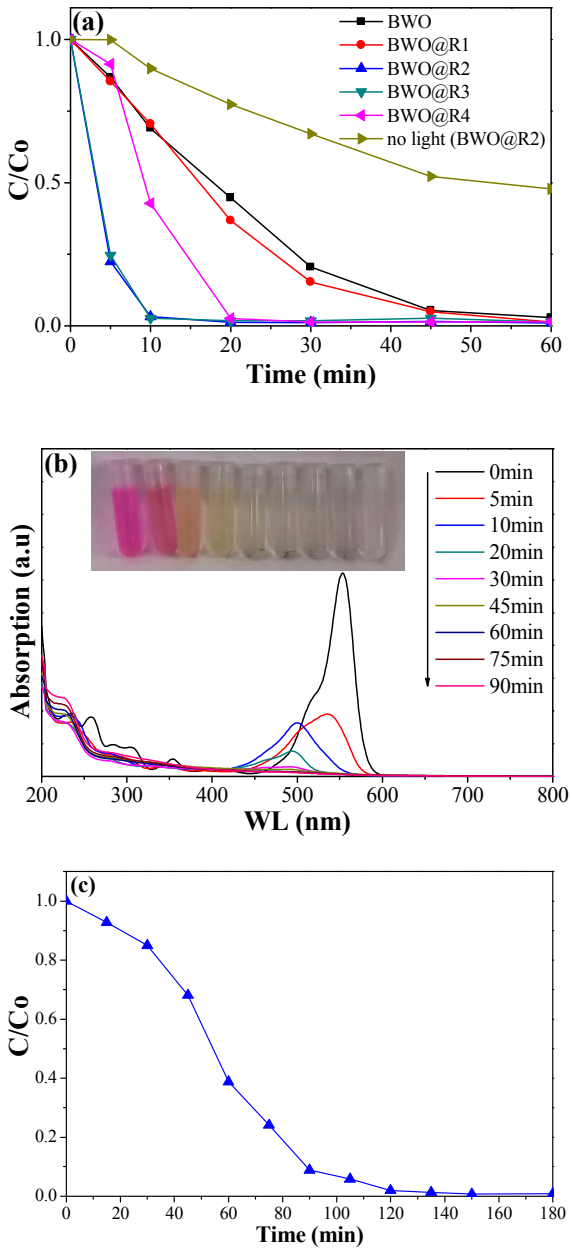


**Figure 9** (a)Photodegradation for RhB with BWO@R composite under visible-light irradiation (BWO@R: 1.00g/L, RhB: $10^{-2}$ g/L); (b)UV-vis spectra of the reaction solution with BWO@R3; (c) Photodegradation for RhB with BWO@R3 under visible-light irradiation (BWO@R: 1.00g/L, RhB: $30^{-2}$ g/L)

To learn the involvement of active radical species in the photocatalytic oxidation of RhB over the as-prepared composite, the electron spin resonance (ESR) analysis were conducted, as shown in Fig. 10. It was obvious that no signals were observed in the dark . With irradiation for 10 min, there were obvious signals for superoxide radical $\cdot O_2^-$(Fig. 10a), indicating that DMPO-$\cdot O_2^-$ species were the main oxidizing species during the period of photodegradation reaction

However, no typical signals with the characteristic intensity of 1 : 2 : 2 : 1 for hydroxyl radical were observed, no matter whether the reaction was conducted in darkness or under light irradiation (Fig. 10b), suggesting that $\cdot OH$ would not be the main oxidizing species of the as-prepared composite in the photodegradation reaction . Previously, similar results have also been reported by Zhou et al.and Wang et al.[46, 47]

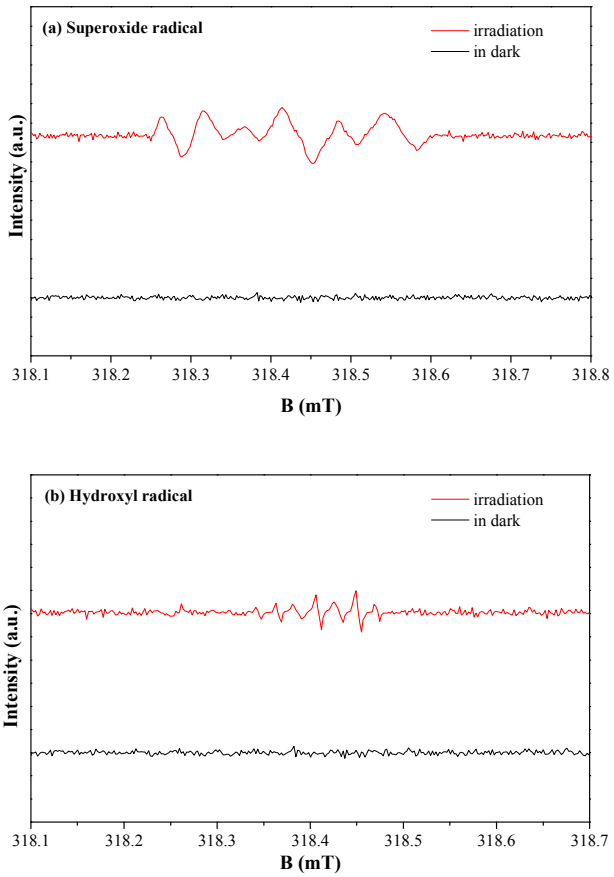


**Figure 10** DMPO spin-trapping ESR spectra of BWO@R3 (a) in methanol dispersion for DMPO-$\cdot O_2^-$and (b) aqueous dispersion for DMPO-$\cdot OH$.

### 3.3 Mechanism of photocatalytic activity enhancement

Based on these experimental results, it is obviously found that the BWO@R exhibitied the enhanced visible-light response and photocatalytic activity on the photodegradation of RhB. These results indicated that the evidently improved photocatalytic property of BWO@R could attributes to its multicomponent composite structure. The loaded RGO not only act as a good substrate and stabilizer of $Bi_2WO_6$/$Bi_2O_3$, but also could efficiently improve the electron transport and reduce charge recombination. Firstly, the potentials of conductance band (CB) and valence band (VB) edges of $Bi_2WO_6$, $Bi_2O_3$ and RGO were investigated. The CB bottoms ($E_{CB}$) and the VB top edge ($E_B$) were calculated empirically according to the formula[48, 49]:

$$E_{CB}=X - E_e-0.5E_g \quad (3)$$

$$E_{VB} = E_g - E_{CB} \quad (4)$$

The results are $E_{CB}$ = 0.46 eV for $Bi_2WO_6$, 0.22 eV for $Bi_2O_3$, and -0.36 eV for RGO[28], respectively. Based on the confirmed forbidden bandwidth of BWO@R (1.72 eV), the corresponding $E_{VB}$ of $Bi_2WO_6$, $Bi_2O_3$ and RGO in the as-prepared composites are determined 2.18, 1.94 and 1.36 eV, respectively. The schematic illustration of the photogenerated carrier transfer and enhanced photocatalytic activity by BWO@R is summarized in Scheme 1.

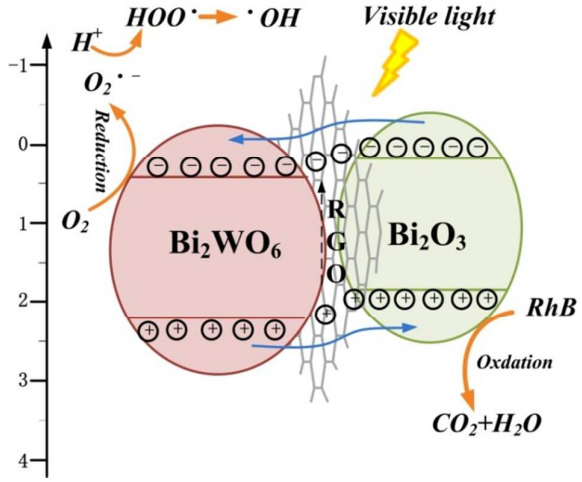


**Scheme 1** Schematic diagram of charge separation in visible-light irradiation and the energy band mechanism of enhanced photocatalytic activity of BWO@R

The main mechanism of the photocatalysis is that the separation of photogenerated carriers is promoted, and then the photogenerated electrons and holes are migrated to the surface of photocatalyst for photocatalytic reaction. The loaded RGO is well blackbody materials which can modify the original formation of photoelectron-hole pairs. In addition, it also broaden the visible-light response range of the prepared heterojuncion, which reduce the forbidden bandwidth. With these improvements, the electrons ($e^-$) in the VB of BWO@R will more easily transit into the CB by the visible-light excitation, which enhances the photogenerated electron-holes separation efficiently. Moreover, RGO serve as an excellent electron acceptor and mediator in this composite material, Photogenerated electrons from $Bi_2WO_6$ and $Bi_2O_3$ could transfer to the large RGO sheets quickly through the presence of the delocalized π electrons[2], which improve the efficiency in separation and migration of photogenerated carrier charge. The effective carrier charge transfer process can inhibit the photogenerated electrons-holes recombination. Thereby, the process can significantly enhance the photocatalytic activity of BWO@R.

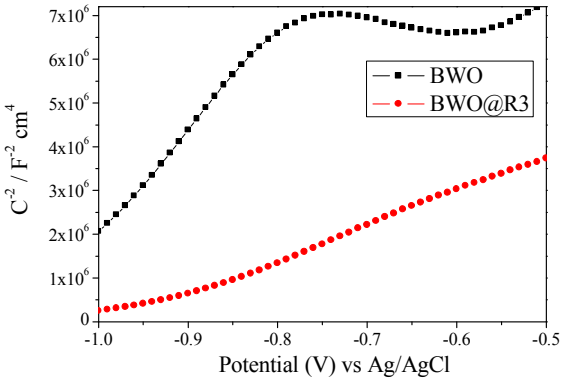


**Figure 10** Mott-Schottky plots of BWO and BWO@R2 composites in 0.5 M $Na_2SO_4$.

To further analyze the reason why the as-prepared composite exhibited enhanced photocatalytic activity under visible-light, Mott–Schottky (MS) measurements were conducted, as shown in Fig. 11. It can be found that both BWO and BWO@R3 show positive slopes, confirming that the composite is mainly typical for n-type semiconductors. Obviously, the $E_{cb}$ of BWO@R3 is more negative than that of BWO, which is in good agreement with the data of theabove-mentioned calculation results[50]. Maeanwhile, it is obvious that the Mott–Schottky plots slope of BOW@R3 is smaller than BWO. It was reported that the smaller slope suggests a faster charge transfer[51]. The Mott-Schottky plots illustrate that charge transfer ability of BWO@R composite is higher than BWO, which contributes to the higher photocatalytic activity of the as-prepared composites[49]. It can futher indicate that loading RGO which owns excellent electron conductivity can reduce band gap of the as-prepared composites and enhance migration of photogenerated carrier charge, so that the as-prepared composite own better visible-light response ability and enhanced visible-light photocatalytic activity.

## Conclusions

In this paper, $Bi_2WO_6/Bi_2O_3$ loaded reduced graphene oxide composite photocatalyst was successfully synthesized via a one-step solvothermal process. It was shown that $Bi_2WO_6/Bi_2O_3$@RGO were synthesized directly from the results of XRD, SEM and EDS. In addition, TEM results determined that multicomponent composites were formed in the composite photocatalyst. In the synthesis process, it was found that GO was completely reduced to graphene and bonded with $Bi_2WO_6/Bi_2O_3$ with by C-O to form BWO@R composite from XPS and FT-IR. BWO@R owned great light absorption from UV to visible-light region and decreased recombination of photogenerated charge carriers, which suggested that the as-prepared composite had the features that can improved photocatalytic performance. The RhB degradation results showed that BWO@R exhibited enhanced photodegration for RhB under visible-light irradiation. Among them, BWO@R3 exhibited the best photocatalytic activity for degradation ratio of RhB reaching 99.6% in 20min. At the same time, it illustrated obviously that loading of graphene significantly enhanced the adsorption of BWO@R3. What is more, these results also

illustrated that the best added GO% for synthesis BWO@R was 2%. Finally, it concludes that RGO serve as an excellent electron acceptor and mediator in the composite which can enhance the migration of photogenerated electrons and inhibit the photogenerated electron-holes recombination. These are the reasons that photocatalytic activity can be enhanced. This work provides not only a principle method to synthesize $Bi_2WO_6$/$Bi_2O_3$ loaded RGO with the excellent photocatalytic performance for actual produce ,but also opens new possibilities to provide some insight into the design of new multicomponent composite of $Bi_2WO_6$ with high photocataly activity, which shows great potential application in energy conversion.

## Acknowledgements

The present work was financially supported by Graduate Innovation Fund of Jilin University(No.2015027), also funded by National Natural Science Foundation of China (Grant No. 41472214) and Jilin Provincial Science & Technology Department (Grant No. 20150204050SF).

## References

1.P. Wang, Y. Ao, C. Wang, J. Hou and J. Qian, *Carbon*, 2012, 50, 5256-5264.

2.S. Sun, W. Wang and L. Zhang, *The Journal of Physical Chemistry C*, 2013, 117, 9113-9120.

3.Y.-L. Min, K. Zhang, Y.-C. Chen and Y.-G. Zhang, *Separation and Purification Technology*, 2012, 86, 98-105.

4.T. Wang, G. Xiao, C. Li, S. Zhong and F. Zhang, *Materials Letters*, 2015, 138, 81-84.

5.Y. Zhou, Z. Tian, Z. Zhao, Q. Liu, J. Kou, X. Chen, J. Gao, S. Yan and Z. Zou, *ACS Applied Materials & Interfaces*, 2011, 3, 3594-3601.

6.Y. Yao, W. Huang, H. Zhou, Y. Zheng and X. Song, *J Nanopart Res*, 2014, 16, 1-9.

7.T. Saison, N. Chemin, C. Chanéac, O. Durupthy, V. r. Ruaux, L. Mariey, F. o. Maugé, P. Beaunier and J.-P. Jolivet, *The Journal of Physical Chemistry C*, 2011, 115, 5657-5666.

8.M.-S. Gui, W.-D. Zhang, Q.-X. Su and C.-H. Chen, *Journal of Solid State Chemistry*, 2011, 184, 1977-1982.

9.W. Wang, Y. Liu, T. L. Li and M. H. Zhou, *Chemical Engineering Journal*, 2014, 242, 1-9.

10.Y.-j. Hao, F.-t. Li, F. Chen, M.-j. Chai, R.-h. Liu and X.-j. Wang, *Materials Letters*, 2014, 124, 1-3.

11.X. Li, R. Huang, Y. Hu, Y. Chen, W. Liu, R. Yuan and Z. Li, *Inorganic Chemistry*, 2012, 51, 6245-6250.

12.P. Zhang, J. Zhang, A. Xie, S. Li, J. Song and Y. Shen, *Rsc Advances*, 2015, 5, 23080-23085.

13.H. Wang, L. Zhang, Z. Chen, J. Hu, S. Li, Z. Wang, J. Liu and X. Wang, *Chemical Society Reviews*, 2014, DOI: 10.1039/C4CS00126E.

14.L. Zhang, W. Wang, M. Shang, S. Sun and J. Xu, *Journal of Hazardous Materials*, 2009, 172, 1193-1197.

15.J. Low, J. G. Yu, Q. Li and B. Cheng, *Physical Chemistry Chemical Physics*, 2013, DOI: 10.1039/C3CP53820F.

16.S. Obregon and G. Colon, *Applied Catalysis B-Environmental*, 2013, 140, 299-305.

17.X. Liu, M. Zhou, G. Yao, W. Shi, C. Ma, P. Lv, Y. Tang and Y. Yan, *Rsc Advances*, 2014, 4, 18264-18269.

18.V. Georgakilas, M. Otyepka, A. B. Bourlinos, V. Chandra, N. Kim, K. C. Kemp, P. Hobza, R. Zboril and K. S. Kim, *Chemical Reviews*, 2012, 112, 6156-6214.

19.J. F. Wang, T. Tsuzuki, B. Tang, L. Sun, X. J. J. Dai, G. D. Rajmohan, J. L. Li and X. G. Wang, *Australian Journal of Chemistry*, 2014, 67, 71-77.

20.B. Z. Tian, T. T. Wang, R. F. Dong, S. Y. Bao, F. Yang and J. L. Zhang, *Applied Catalysis B-Environmental*, 2014, 147, 22-28.

21.T. Som, G. V. Troppenz, R. R. Wendt, M. Wollgarten, J. Rappich, F. Emmerling and K. Rademann, *Chemsuschem*, 2014, 7, 854-865.

22.H. Lv, Y. Liu, J. Hu, Z. Li and Y. Lu, *Rsc Advances*, 2014, 4, 63238-63245.

23.J. Zhang, Z.-H. Huang, Y. Xu and F. Kang, *Journal of the American Ceramic Society*, 2013, 96, 1562-1569.

24.Z. Sun, J. Guo, S. Zhu, L. Mao, J. Ma and D. Zhang, *Nanoscale*, 2014, 6, 2186-2193.

25.H. Ma, J. Shen, M. Shi, X. Lu, Z. Li, Y. Long, N. Li and M. Ye, *Applied Catalysis B: Environmental*, 2012, 121–122, 198-205.

26.J. Low, J. Yu, Q. Li and B. Cheng, *Physical Chemistry Chemical Physics*, 2014, 16, 1111-1120.

27.J. Xu, Y. Ao and M. Chen, *Materials Letters*, 2013, 92, 126-128.

28.E. Gao, W. Wang, M. Shang and J. Xu, *Physical chemistry chemical physics : PCCP*, 2011, 13, 2887-2893.

29.Y. Fu, C. Chang, P. Chen, X. Chu and L. Zhu, *Journal of Hazardous Materials*, 2013, 254–255, 185-192.

30.J. Cao, B. Xu, H. Lin, B. Luo and S. Chen, *Dalton transactions*, 2012, 41, 11482-11490.

31.M.-S. Gui and W.-D. Zhang, *Journal of Physics and Chemistry of Solids*, 2012, 73, 1342-1349.

32.X.-T. Wang, R. Lv and K. Wang, *Journal of Materials Chemistry A*, 2014, DOI: 10.1039/c4ta00696h.

33.G. Zhang, F. Lü, M. Li, J. Yang, X. Zhang and B. Huang, *Journal of Physics and Chemistry of Solids*, 2010, 71, 579-582.

34.H. Guo, Y. Guo, L. Liu, T. Li, W. Wang, W. Chen and J. Chen, *Green Chemistry*, 2014, DOI: 10.1039/c4gc00065j.

35.M. Maczka, J. Hanuza, W. Paraguassu, A. G. Souza, P. T. C. Freire and J. Mendes Filho, *Applied Physics Letters*, 2008, 92.

36.F. Chen, Y. Cao and D. Jia, *Journal of Colloid and Interface Science*, 2013, 404, 110-116.

37.P. Ju, P. Wang, B. Li, H. Fan, S. Ai, D. Zhang and Y. Wang, *Chemical Engineering Journal*, 2014, 236, 430-437.

38.X. Huang and H. Chen, *Applied Surface Science*, 2013, 284, 843-848.

39.P. Ju, P. Wang, B. Li, H. Fan, S. Ai, D. Zhang and Y. Wang, *Chemical Engineering Journal*, 2014, 236, 430-437.

40.Z. Zhang, W. Wang, L. Wang and S. Sun, *ACS applied materials & interfaces*, 2012, 4, 593-597.

41.D. K. Ma, M. L. Guan, S. S. Liu, Y. Q. Zhang, C. W. Zhang, Y. X. He and S. M. Huang, *Dalton transactions*, 2012, 41, 5581-5586.

42.F.-J. Zhang, F.-Z. Xie, J. Liu, W. Zhao and K. Zhang, *Ultrasonics Sonochemistry*, 2013, 20, 209-215.

43.M. Shang, W. Wang and H. Xu, *Crystal Growth & Design*, 2008, 9, 991-996.

44.J. Zhuang, W. Dai, Q. Tian, Z. Li, L. Xie, J. Wang, P. Liu, X. Shi and D. Wang, *Langmuir*, 2010, 26, 9686-9694.

45.K. Yu, S. Yang, H. He, C. Sun, C. Gu and Y. Ju, *The Journal of Physical Chemistry A*, 2009, 113, 10024-10032.

46.Y. Zhou, X. Zhang, Q. Zhang, F. Dong, F. Wang and Z. Xiong, *Journal of Materials Chemistry A*, 2014, 2, 16623-16631.

47.C. Wang, L. Zhu, M. Wei, P. Chen and G. Shan, *Water Research*, 2012, 46, 845-853.

48.Z.-Q. Li, X.-T. Chen and Z.-L. Xue, *Journal of Colloid and Interface Science*, 2013, 394, 69-77.

49.J. Yan, G. Wu, N. Guan and L. Li, *Applied Catalysis B: Environmental*, 2014, 152–153, 280-288.

50.T. Wang, F. Zhang, G. Xiao, S. Zhong and C. Lu, *Photochem. Photobiol.*, 2015, 91, 291-297.

51.F. Su, T. Wang, R. Lv, J. Zhang, P. Zhang, J. Lu and J. Gong, *Nanoscale*, 2013, 5, 9001-9009.

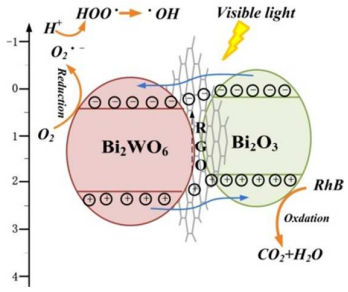


Schematic diagram of charge separation in visible-light irradiation and the energy band mechanism of enhanced photocatalytic activity of BWO@R